Journal of Coordination Chemistry

ISSN: 0095-8972 (Print) 1029-0389 (Online) Journal homepage: http://www.tandfonline.com/loi/gcoo20

A bulky oxime for the synthesis of Mn(III) clusters

Dimitris A. Kalofolias, Andreas G. Flamourakis, Milosz Siczek, Tadeusz Lis & Constantinos J. Milios

To cite this article: Dimitris A. Kalofolias, Andreas G. Flamourakis, Milosz Siczek, Tadeusz Lis & Constantinos J. Milios (2015) A bulky oxime for the synthesis of Mn(III) clusters, Journal of Coordination Chemistry, 68:19, 3472-3484, DOI: 10.1080/00958972.2015.1075014

To link to this article: http://dx.doi.org/10.1080/00958972.2015.1075014

Accepted author version posted online: 24 Jul 2015.
Published online: 17 Aug 2015.

Journal of Coordination Chemistry, 2015
Vol. 68, No. 19, 3472–3484, http://dx.doi.org/10.1080/00958972.2015.1075014

A bulky oxime for the synthesis of Mn(III) clusters

DIMITRIS A. KALOFOLIAS†, ANDREAS G. FLAMOURAKIS†, MILOSZ SICZEK‡, TADEUSZ LIS‡ and CONSTANTINOS J. MILIOS*†

†Department of Chemistry, University of Crete, Herakleion, Greece
‡Faculty of Chemistry, University of Wroclaw, Wroclaw, Poland

(*Received 3 April 2015; accepted 30 June 2015*)

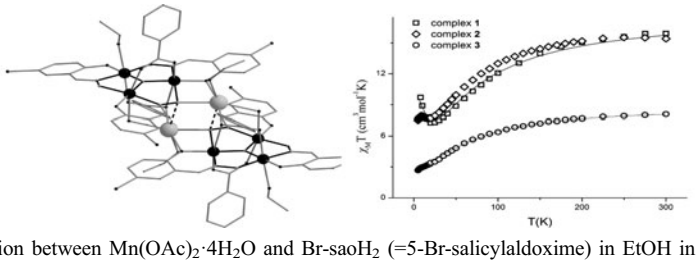

The reaction between $Mn(OAc)_2{\cdot}4H_2O$ and Br-saoH$_2$ (=5-Br-salicylaldoxime) in EtOH in the presence of NMe_4OH led to the formation of the hexanuclear cluster $[Mn_6O_2(Br\text{-}sao)_6(OAc)_2(H_2O)_2(EtOH)_2]{\cdot}2.8H_2O{\cdot}2.2EtOH$ (**1**). Switching from $Mn(OAc)_2{\cdot}4H_2O$ to $Mn(ClO_4)_2{\cdot}6H_2O$, the same reaction upon addition of pivH (= trimethyl acetic acid) yielded $[Mn_6O_2(Br\text{-}sao)_6(piv)_2(H_2O)_2(EtOH)_2]{\cdot}6EtOH$ (**2** 6EtOH), and finally upon changing pivH to NaO_2CPh, we were able to isolate $[Mn_6Na_2O_2(Br\text{-}sao)_6(O_2CPh)_4(H_2O)_2(EtOH)_4]{\cdot}6EtOH$ (**3** 6EtOH). Clusters **1** and **2** 6EtOH describe "typical" [Mn_6/oximate] complexes consisting of two {Mn_3} oxo-centered triangular units bridged by oximate groups, while in **3** 6EtOH these triangular motifs are separated by two sodium cations. An investigation into the magnetic properties of all three clusters revealed the presence of dominant antiferromagnetic interactions, leading to ground states of $S = 4$ and 2 for **1** and **3**, respectively. Finally, cluster **2** 6EtOH functions as a single-molecule magnet with $U_{eff} = 27.54$ K.

Keywords: Mn(III) oximato complexes; Crystal structures; Magnetic properties; Single-molecule magnets

1. Introduction

Manganese oximate cluster chemistry has witnessed an enormous growth during the last decade; initially started in 1998 by Chaudhuri reporting on the synthesis of the hexanuclear Mn(III) cluster $[Mn^{III}_6O_2(O_2CPh)_2(sao)_6(H_2O)_2(MeCN)_2]$ (saoH$_2$ = salicylaldoxime) [1], and was followed by the same group reporting the synthesis of the dinuclear complex $[Mn^{III}_2(sao)_3(tmtacn)]$ (tmtacn = 1,4,7-trimethyl-1,4,7-triazacyclononane) [2]. It expanded exponentially upon the synthesis and characterization of a series of polymetallic $[Mn^{III}_x]$ clusters, especially for $x = 6$ [3–36] and $x = 3$ [37–50]. Furthermore, for the former family

*Corresponding author. Email: komil@chemistry.uoc.gr

of compounds with general formula $[Mn_6^{III}O_2(R\text{-sao})_6(O_2CR)_2(L)_{4-6}]$ (R=H, CH_3, CH_2–CH_3, Ph; L = solvent), it was found that the vast majority of the products could function as single-molecule magnets (SMMs) retaining their magnetization, once magnetized, in the absence of an external magnetic field. In addition, for this family, the ground state, S, of each cluster is strongly dependent on the Mn–N–O–Mn torsion angles present in the metallic core of the complex, and as such, values ranging from $S = 4$ to $S = 12$ were established, affecting the properties of the SMM.

More than 30 $[Mn_6^{III}O_2(R\text{-sao})_6(O_2CR)_2(L)_{4-6}]$ clusters have been isolated featuring various substituted salicyl-like oximate and carboxylate ligands. The astonishing feature of all of these clusters is the fact that all of them obey the "magic area" rule [10] which allows us to predict the sign of the magnetic-exchange interaction, J, within any Mn_2^{III} pair bridged by an oximate –N–O– group. According to that rule, there is an area of 30.4–31.3° regarding the Mn–N–O–Mn torsion angle, α; if $\alpha < 30.4°$, then $J < 0$ (AF), and if $\alpha > 31.3°$, then $J > 0$ (F). While this rule has been successfully tested upon all substituted salicyl-like oximate ligands carrying substituents on the oximic carbon used so far (Me-saoH, Et-saoH, Ph-saoH), it has never been tested against oxime ligands that carry substituents on the aromatic ring. Therefore, in this work, we present our initial results upon employing 5-bromo-salicylaldoxime, Br-saoH$_2$ (scheme 1), in manganese cluster chemistry, as a means of: (i) expanding the $[Mn_6^{III}$/oximate] family, (ii) investigating the effect of placing the bulky substituent on the aromatic oxime ring on the identity of the products, and (iii) testing the validity of the "magic area" rule for a new type of substituted oxime ligand.

2. Experimental

2.1. *General and physical measurements*

All manipulations were performed under aerobic conditions using materials as received (reagent grade). *Caution*! Although we encountered no problems, care should be taken when using the potentially explosive perchlorate ion. Br-saoH$_2$ was synthesized by the reaction of the precursor aldehyde with hydroxylamine and sodium acetate in EtOH, as described [51]. Elemental analyses (C, H, and N) were performed by the EaStCHEM

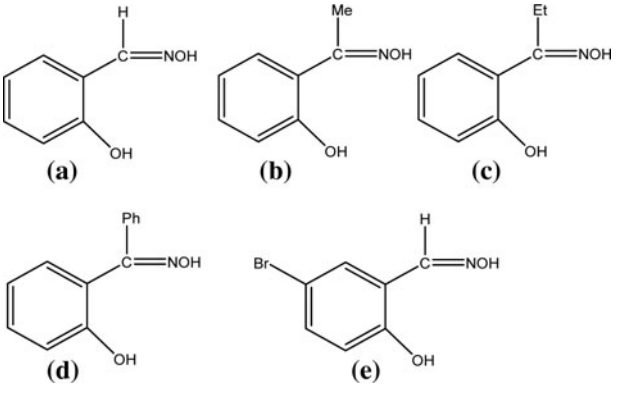

Scheme 1. Ligands discussed in the text; top left to bottom right: (a) saoH$_2$, (b) Me-saoH$_2$, (c) Et-saoH$_2$, (d) Ph-saoH$_2$, (e) Br-saoH$_2$.

microanalysis service. Variable-temperature, solid-state direct-current (dc) magnetic susceptibility data down to 5 K were collected on a Quantum Design MPMS-XL SQUID magnetometer equipped with a 7-T dc magnet at the U. Crete. Diamagnetic corrections were applied to the observed paramagnetic susceptibilities using Pascal's constants.

2.2. *Compound preparation*

2.2.1. Synthesis of $[Mn_6O_2(Br\text{-}sao)_6(OAc)_2(H_2O)_2(EtOH)_2]\cdot 2.8H_2O\cdot 2.2EtOH$ (1·2.8H_2O·2.2EtOH) (1). $Mn(OAc)_2\cdot 4H_2O$ (245 mg, 1.0 mmol), and Br-saoH_2 (216 mg, 1.0 mmol) were dissolved in EtOH (15 mL) in the presence of NMe_4OH (1.0 mmol), and the resulting green solution was stirred for 45 min. The dark green solution formed was filtered and left undisturbed to evaporate slowly. After ~1 day, dark-green crystals of **1** 2.8H_2O·2.2EtOH were obtained in ~40% yield (based on Mn; 133 mg). The crystals were isolated by vacuum filtration, washed with diethyl ether (2 × 5 mL), and dried in air. Anal. Calcd for $[Mn_6O_2(Br\text{-}sao)_6(OAc)_2(H_2O)_2(EtOH)_2]\cdot 2H_2O$ ($C_{50}H_{50}Br_6Mn_6N_6O_{24}$): C 31.15, H 2.61, N 4.36%. Found C 31.08, H 2.47, N 4.29%; selected IR data (KBr): ν = 1590m, 1528m, 1459s, 1398s, 1273vs, 1180s, 1131m, 1028vs, 1010vs, 816s, 705vs, 662vs, 646vs, 471vs.

2.2.2. Synthesis of $[Mn_6O_2(Br\text{-}sao)_6(piv)_2(H_2O)_2(EtOH)_2]\cdot 6EtOH$ (2·6EtOH) (2). $Mn(ClO_4)_2\cdot 6H_2O$ (361 mg, 1.0 mmol), Br-saoH_2 (216 mg, 1.0 mmol), and pivH (204 mg, 2.0 mmol) were stirred in EtOH (20 mL) for 5 min, followed by addition of NMe_4OH (1.0 mmol). The solution was further stirred for ~30 min to yield a dark-green solution, which was filtered and left to evaporate at room temperature. Dark-green crystals of **2** 6EtOH were formed after ~2 days in ~45% yield (based on Mn; 164 mg). The crystals were isolated by vacuum filtration, washed with diethyl ether (2 × 10 mL), and dried in air. Anal. Calcd for $[Mn_6O_2(Br\text{-}sao)_6(piv)_2(H_2O)_2(EtOH)_2]\cdot 3EtOH$ ($C_{62}H_{76}$ $Br_6Mn_6N_6O_{25}$): C 35.22, H 3.62, N 3.97%. Found C 34.99, H 3.54, N 3.82%; selected IR data (KBr): ν = 1589m, 1518m, 1457s, 1395s, 1276vs, 1179s, 1133m, 1030vs, 1010vs, 820s, 814s, 704vs, 660vs, 644vs, 471vs.

2.2.3. Synthesis of $[Mn_6Na_2O_2(Br\text{-}sao)_6(O_2CPh)_4(H_2O)_2(EtOH)_4]\cdot 6EtOH$ (3·6EtOH) (3). $Mn(ClO_4)_2\cdot 6H_2O$ (361 mg, 1.0 mmol), Br-saoH_2 (216. mg, 1.0 mmol), NaO_2CPh (288 mg, 2.0 mmol), and NMe_4OH (1.0 mmol) were added in EtOH (20 mL) and the resulting solution was stirred for a total of 40 min. The solution was filtered and left undisturbed at room temperature to evaporate slowly. After ~1 day dark-green crystals of **3** 6EtOH were obtained in ~55% yield (based on Mn; 232 mg). The crystals were isolated by vacuum filtration, washed with diethyl ether (2 × 5 mL), and dried in air. Anal. Calcd for $[Mn_6Na_2O_2(Br\text{-}sao)_6(O_2CPh)_4(H_2O)_2(EtOH)_4]\cdot 3EtOH$ $C_{84}H_{90}Br_6Mn_6N_6Na_2O_{31}$: C 40.02, H 3.75, N 3.26%. Found C 39.91, H 3.49, N 3.13%; selected IR data (KBr): ν = 1587m, 1528m, 1457s, 1397s, 1370s, 1274vs, 1178s, 1134m, 1031vs, 819s, 703vs, 659vs, 635vs, 463vs.

2.3. *Single-crystal X-ray crystallography*

Diffraction data for **1** 2.8H_2O·2.2EtOH, **2** 6EtOH, and **3** 6EtOH were collected at 100, 80, and 80 K, respectively on an Xcalibur R four-circle diffractometer with a Ruby CCD

Table 1. Crystal and structure refinement data for **1**–**3**.

Compound reference	**1**	**2**	**3**
Chemical formula	$C_{54.40}H_{64.80}Br_6Mn_6N_6O_{27}$	$C_{68}H_{94}Br_6Mn_6N_6O_{28}$	$C_{86}H_{96}Br_6Mn_6N_6Na_2O_{32}$
Formula mass	2043.82	2252.59	2580.76
Crystal system	Monoclinic	Triclinic	Triclinic
a (Å)	28.84 (3)	11.916 (4)	13.536 (5)
b (Å)	17.78(12)	13.008 (5)	14.010 (5)
c (Å)	18.52 (2)	14.681 (5)	14.238 (5)
α (°)		104.86 (4)	74.39 (3)
β (°)	127.41 (4)	93.40 (3)	72.08 (4)
γ (°)		96.71 (3)	82.10 (4)
Unit cell volume (Å)^3	7543 (13)	2175.0 (14)	2469.9 (17)
Temperature (K)	100	80	80
Space group	*C2/c*	*P-1*	*P-1*
No. of formula units per unit cell (*Z*)	4	1	1
Radiation type	Mo-Kα	Mo-Kα	Mo-Kα
Absorption coefficient (μ/mm^{-1})	4.23	3.68	3.26
No. of reflections measured	12,692	14,454	16,311
No. of independent reflections	6919	9448	11,296
R_{int}	0.108	0.058	0.057
Final R_1 values [$I > 2\sigma(I)$]	0.086	0.070	0.074
Final R_1 values (all data)	0.188	0.142	0.148
Final *wR* (F^2) values (all data)	0.138	0.090	0.118
Goodness of fit on F^2	1.00	0.99	1.00
CCDC	1,051,160	1,051,161	1,051,162

detector. The structures were solved by direct methods with SHELXS and refined by full-matrix least-squares techniques on F^2 with SHELXL [52]. The hydrogens were included in idealized geometry riding on their parent atoms with C–H = 0.95–0.99 Å, and with U_{iso}(H) = 1.2U_{eq}(CH, CH_2) or 1.5U_{eq}(CH_3), except for water hydrogens, which were located in the Fourier maps, refined with O–H distances restrained to 0.840(1) Å and then constrained to parent atoms (AFIX 3 instruction). The site occupancy factors of uncoordinated ethanol and water molecules in **1** were refined and at the final stage of refinement cycles were fixed at s.o.f. = 0.7 (for O2E), 0.4 (for O3E), 0.6 (for O2W), 0.2 (for O3W), 0.3 (for O4W), 0.2 (for O5W) and 0.1 (for O6W). The Br from one of the ligands is disordered over two sites and was refined with s.o.f. = 0.621(15) and 0.379(15). One coordinated and two uncoordinated ethanol molecules in **2** are disordered over two sites and refined with s.o.f. = 0.777 (12) and 0.223(12) for O1E; 0.747(6) and 0.253(6) for O1G; and 0.8 and 0.2 for O1H. The hydrogens from disordered water molecules were not found. Data collection parameters and structures solution and refinement details are listed in table 1.

3. Results and discussion

3.1. *Syntheses*

Complexes **1**–**3** were obtained following the "typical" procedure for the [Mn_6/oximate] clusters reported [21], according to which a Mn(II) salt, usually $Mn(ClO_4)_2{\cdot}6H_2O$, reacts with the oxime ligand in basic alcoholic solutions in the presence of various carboxylates. In all three clusters, the manganese centers were found in the 3+ oxidation state, while the starting manganese material contained exclusively divalent manganese ions. This oxidation process is very common in manganese chemistry, and is most likely due to the presence of

atmospheric dioxygen. For all three complexes, the nature of the base does not affect the identity of the products since upon changing NMe_4OH to either NEt_3 or NEt_4OH, we did not manage to isolate any other crystalline products besides **1**–**3**, as verified by IR and pXRD measurements. In addition, repeating the reactions under solvothermal conditions led to an amorphous yellow-orange precipitate, which could not be identified further. Complexes **1** and **2** display the same structural motif and general formulas, while **3** incorporates two sodium cations into its structure due to the use of NaO_2CPh as the carboxylate source. Attempts to use $PhCO_2H$ or $Mn(O_2CPh)_2{\cdot}2H_2O$ as the carboxylate source, and therefore to obtain the benzoate analog of **1** or **2**, have so far proven fruitless.

3.2. *Description of structures*

Complex **1** crystallizes in the monoclinic space group *C2/c*, while **2** crystallizes in the triclinic *P-1* space group. Both **1** and **2** display similar structures; two oximate oxo-centered triangular $[Mn^{III}_3(\mu_3\text{-}O)(\text{–}N_{ox}\text{–}O_{ox}\text{–})_3]^{4+}$ building blocks (figure 1, left) are arranged in an off-set fashion linked via two $O_{oximate}$ atoms, each one belonging to a $[Mn_3]$ subunit, resulting in a $[Mn^{III}_6O_2(\text{–}N_{ox}\text{–}O\text{–}_{ox})_6]^{8+}$ unit. Furthermore, on each $[Mn_3]$ subunit, a capping carboxylate is present in an $\eta^1:\eta^1:\mu$ coordination mode, thus forming a $[Mn^{III}_6O_2(\text{–}N_{ox}\text{–}O\text{–}_{ox})_6(O_2CR)_2]^{6+}$ metallic core (figure 1, right). All oximate ligands present in the structure are doubly deprotonated, Br-sao^{2-}; four ligands are found in an $\eta^1:\eta^1:\eta^1:\mu$-fashion (scheme 2) forming a chelate six-member ring via the $O_{aromatic}$ and $N_{oximate}$, while the remaining two, responsible for the inter-triangular linkage, are found in an $\eta^2:\eta^1:\eta^1:\mu_3$-fashion. The coordination environment is completed by two terminal H_2O molecules and two solvent molecules. All manganese centers are in 3+ oxidation state; four manganese centers are six-coordinate adopting a *JT* distorted octahedral geometry with an O_5N coordination sphere, while the remaining two are five-coordinate adopting square pyramidal geometry with an O_4N coordination sphere.

In the crystal lattice, **1** adopts a *zigzag* conformation along the *c*-axis of the unit cell (figure 2, left) in which the hexanuclear units are connected via intermolecular hydrogen bonds between the oxime and solvent molecules coordinated at the Mn3 of each

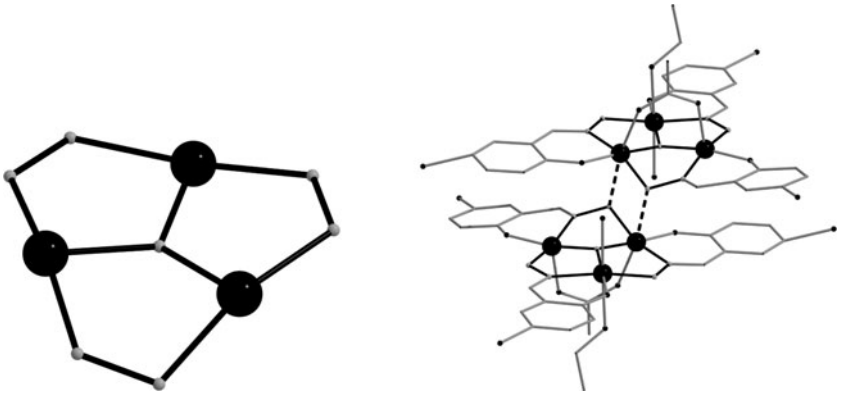

Figure 1. The $[Mn^{III}_3(\mu_3\text{-}O)(\text{-}N_{ox}\text{-}O_{ox}\text{-})_3]^{4+}$ building block of **1** and **2** (left); the general $[Mn^{IIII}_6O_2(Br\text{-}sao)_6(O_2CR)_2(H_2O)_2(EtOH)_2]^{6+}$ molecular structure for **1** and **2** (right). Hydrogens and co-crystallized solvent molecules are omitted for clarity.

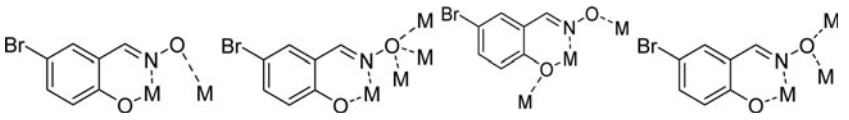

Scheme 2. The different coordination modes of the Br-sao^{2-} ligands in all three complexes. See text for details.

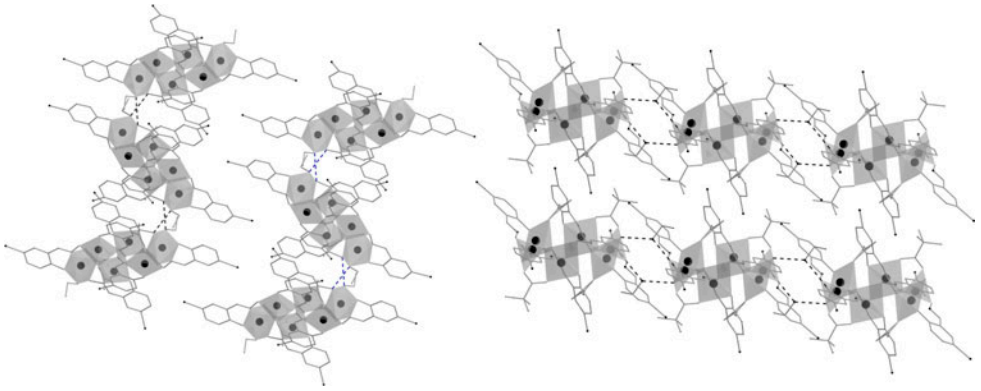

Figure 2. *Zigzag* conformation in the crystal lattice of **1** (left); crystal packing of **2** (right).

hexanuclear unit (O1E···O1A^{i}). For **2**, the crystal lattice consists of sheets along the *b*-axis (figure 2, right) stabilized by both intramolecular and intermolecular hydrogen bonds; the former are formed between the $O_{aromatic}$ and the ethanol molecules (O1E···O1A^{ii}), while the latter occur between co-crystallized solvent molecules and the oximate ligands (O1F···O1B; O1W···O1F^{iv}).

Complex **3** crystallizes in the triclinic *P-1* space group (figure 3); even though it still consists of two carboxylate capped $[Mn^{III}_3(\mu_3\text{-}O)(\text{–}N_{ox}\text{–}O_{ox}\text{–})_3]^{4+}$ building blocks as **1** and **2**, these two blocks are now "separated" by two sodium cations to form a $[Mn^{III}_6Na_2O_2(\text{Br-sao})_6(O_2CR)_4]^{6+}$ core. Each Na^+ is held in place by one bridging water molecule, one

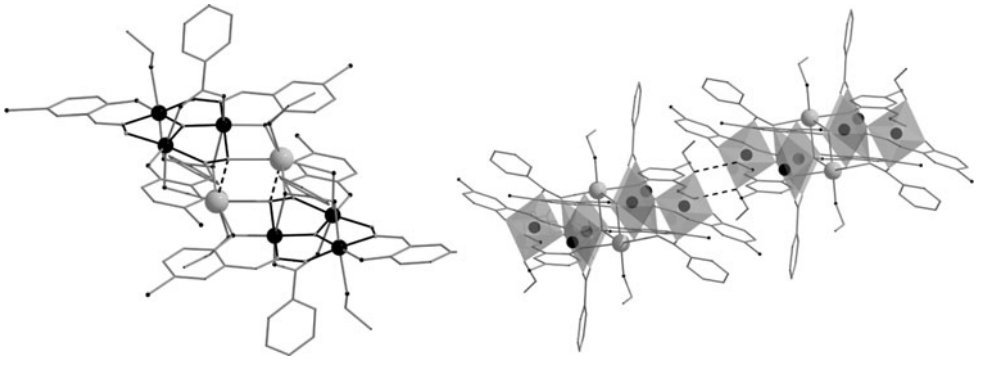

Figure 3. The molecular structure of **3** (left); hydrogen bonds for **3**. Hydrogens and co-crystallized solvent molecules are omitted for clarity.

additional carboxylate, two μ_3-$O_{oximate}$ and one bridging monoatomic O_R alkoxide, while its "coordination" sphere is completed by a terminal EtOH molecule, thus adopting an "octahedral" geometry based on purely ionic interactions. The oximate ligands are all doubly deprotonated and adopt three different coordination modes: (i) two are found in an $\eta^1:\eta^1:\eta^1:\mu$-fashion, (ii) two in an $\eta^3:\eta^1:\eta^1:\mu_4$-fashion and (iii) two in an $\eta^2:\eta^1:\eta^1:\mu_3$ mode, with the former four species responsible for the Na^+ binding. In the crystal lattice, **3** forms sheets along the *b*-axis of the unit cell (figure 3, right); the structure is stabilized by five types of O–H···O intramolecular H-bonds (O17···O24^{ii}; O1W···O18; O18···O19; O19···O12; O1W···O15); in addition, the supramolecular structure is stabilized by H-bonding between the oximate and solvate ethanol molecules (O16···O23^{iv}) (table 2).

3.3. *Magnetic properties*

Direct-current magnetic susceptibility studies were performed on polycrystalline samples of **1**–**3** in the 5-300 K range under an applied field of 0.1 T. The results are plotted as the $\chi_M T$ product *versus* *T* in figure 4. All complexes display similar behavior; the $\chi_M T$ decreases upon cooling, suggesting the presence of dominant antiferromagnetic and/or competing interactions. For all clusters, the room temperature $\chi_M T$ values were found very close to the theoretical values expected for six non-interacting Mn^{III} ions ($g = 2.00$) for **1** and **2**, and three non-interacting Mn^{III} ions ($g = 2.00$) for **3**. For **1,** the room temperature $\chi_M T$ value of 15.83 $cm^3\ mol^{-1}$ K (theoretical value of 18 $cm^3\ mol^{-1}$ K) decreases upon cooling until it

Table 2. Hydrogen-bond geometry (Å, º).

D–H···*A*	*D*–H	H···*A*	*D*···*A*	*D*–H···*A*
1				
O1*E*–H1*E*···O1*A*^{i}	0.84	2.09	2.929 (9)	176
O2*E*–H2*E*···O2*D*^{iii}	0.84	2.14	2.918 (15)	154
O3*E*–H3*E*···O2*W*	0.84	1.69	2.48 (3)	157
O1*W*–H1*W*1···O2*A*^{ii}	0.84	2.38	3.184 (9)	159
O1*W*–H1*W*1···O1*B*^{ii}	0.84	2.47	3.111 (8)	134
O1*W*–H1*W*2···O2*W*^{ii}	0.84	2.28	2.814 (14)	121
O1*W*–H1*W*2···O5*W*^{ii}	0.84	2.00	2.71 (4)	142
O1*W*–H1*W*2···O6*W*^{ii}	0.84	2.43	3.14 (8)	143
2				
O1*W*–H1*W*···O1*H*	0.86	1.98	2.831 (8)	168
O1*W* – H1*W*···O1*HH*	0.86	1.85	2.64 (4)	152
O1*W*–H2*W*···O1*F*^{iv}	0.86	1.85	2.703 (6)	170
O1*E*–H1*EE*···O1*A*^{ii}	0.84	2.18	2.995 (6)	163
O1*E*–H1*E*···O2*B*^{ii}	0.84	2.58	3.095 (5)	121
O1*E*–H1*EE*···O1*A*^{ii}	0.84	2.18	2.995 (6)	163
O1*E*–H1*E*···O2*B*^{ii}	0.84	2.58	3.095 (5)	121
O1*F*–H1*F*···O1*B*	0.86	2.17	2.930 (5)	148
O1*F*–H1*F*···O2*C*	0.86	2.44	3.183 (6)	146
O1*G*–H1*G*···O1*C*	0.84	1.98	2.803 (8)	165
3				
O16–H161···O23^{iv}	0.86	1.90	2.711 (6)	157
O17–H171···O24^{ii}	0.86	1.92	2.769 (6)	167
O1*W*–H1*W*1···O18	0.99	1.87	2.735 (6)	144
O1*W*–H1*W*2···O15	0.99	1.88	2.675 (5)	136
O18–H1*H*···O19	0.84	1.83	2.671 (7)	179
O19–H1*I*···O12	0.84	2.01	2.784 (7)	154

Symmetry codes: (i) $-x+1$, y, $-z+3/2$; (ii) $-x+1$, $-y+1$, $-z+1$; (iii) $-x+1/2$, $y-1/2$, $-z+½$ and (iv) $-x+1$, $-y$, $-z+1$.

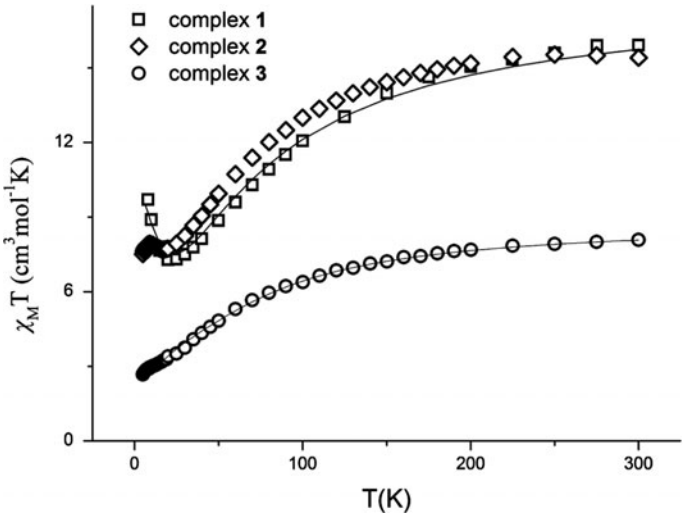

Figure 4. $\chi_M T$ *vs.* T plot for **1**, **2,** and **3** under an applied dc field of 1000 G. The solid lines represent the fit of the data in the 5–300-K range (see text for details).

reaches the minimum value of 7.24 cm^3 mol^{-1} K at 26 K, below which it increases to the final value of 9.71 cm^3 mol^{-1} K at 5 K. For **2**, the room temperature $\chi_M T$ value of 15.32 cm^3 mol^{-1} K slightly decreases upon cooling until ~180 K, before it drops to a minimum value of 7.69 cm^3 mol^{-1} K at 20 K, below which a small "bump" is observed leading to the minimum value of 7.51 cm^3 mol^{-1} K at 5 K. Finally, for **3,** the room temperature $\chi_M T$ value of 8.07 cm^3 mol^{-1} K (theoretical value of 9.00 cm^3 mol^{-1} K) decreases slightly upon cooling until ~170 K, before it drops to the minimum value of 2.67 cm^3 mol^{-1} K at 5 K.

We were able to fit the data for **1** and **3**, adopting a 3-*J* and a 2-*J* model, respectively (figure 5). More specifically, for **1,** we assumed one J_1 interaction between (i) Mn1–Mn3

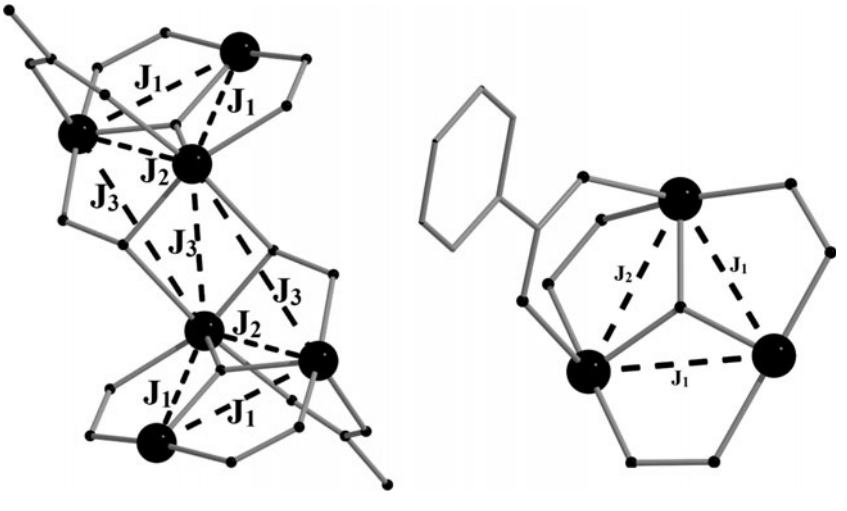

Figure 5. Exchange interaction schemes for complexes **1** (left) and **3** (right).

(and their symmetry related equivalent ions) mediated by a μ_3-oxo bridge and an oximate ligand with a Mn–N–O–Mn torsion angle of 1.4(8)°, and (ii) Mn3–Mn2 (and their symmetry related equivalent ions) mediated by the μ_3-oxo bridge and an oximate ligand with a Mn–N–O–Mn torsion angle of −1.3(9)°, one J_2 interaction between Mn1 and Mn2, as well as their symmetry-related metal centers, mediated by the μ_3-oxo bridge, an oximate ligand with a Mn–N–O–Mn torsion angle of 29.9(8)° and the *syn,syn*– $\eta^1:\eta^1:\mu$ acetate, and one J_3 responsible for the inter-triangular [Mn_3] linkage between Mn1–$Mn1^{ii}$, Mn2–$Mn1^{ii}$, and Mn1–$Mn2^{ii}$ (ii = $1-x$, $1-y$, $1-z$). Using the program *Phi* [53] and the Hamiltonian in equation (1)

$$\hat{H} = -2J_1(\hat{S}_1\hat{S}_3 + \hat{S}_3\hat{S}_2 + \hat{S}_1'\hat{S}_3' + \hat{S}_3'\hat{S}_2') - 2J_2(\hat{S}_1\hat{S}_2 + \hat{S}_1'\hat{S}_2') - 2J_3(\hat{S}_1\hat{S}_1' + \hat{S}_2\hat{S}_1' + \hat{S}_2'\hat{S}_1) \quad (1)$$

afforded the parameters $J_1 = -4.6\ cm^{-1}$, $J_2 = -1.8\ cm^{-1}$, $J_3 = +1.25\ cm^{-1}$, and $g = 1.98$. These parameters lead to an $S = 4$ ground state, with the first excited state of $S = 2$ located ~7 cm^{-1} above (figure 6, left). All J values obtained are in full agreement with the proposed "torsion's angles" rule; both J_1 and J_2 are AF, since the torsion angle is below the limit of ~30.3°, while in addition J_2 is very weak, yet AF, since the corresponding torsion angle is on the borderline of the "magic area". Finally, J_3 was found F as is the case for all [Mn_6] clusters reported so far.

For **3,** we adopted a 2-J model; one J_1 interaction between (i) Mn1–Mn2 mediated by one oximate ligand with a Mn–N–O–Mn torsion angle of 19.2(5)°, and (ii) Mn3–Mn1 mediated by an oximate ligand with a Mn–N–O–Mn torsion angle of −6.3(6)°, and one J_2 exchange interaction between Mn2 and Mn3 mediated via the *syn,syn*– $\eta^1:\eta^1:\mu$ benzoate and an oximate ligand with a torsion Mn–N–O–Mn angle of −25.9(5)°. Using the *Phi* program [53] and the Hamiltonian in equation (2)

$$\hat{H} = -2J_1(\hat{S}_1\hat{S}_2 + \hat{S}_1\hat{S}_3) - 2J_2(\hat{S}_2\hat{S}_3) \quad (2)$$

yielded the parameters $J_1 = -1.0\ cm^{-1}$, $J_2 = -6.1\ cm^{-1}$, and $g = 1.98$. These parameters lead to an $S = 2$ ground state with the first excited $S = 1$ located ~6 cm^{-1} above (figure 6, right), and are in excellent agreement with previously reported values for type I ([$Mn_3^{III}O$(R-sao)$_3$(X)(sol)$_{3-4}$] (R=H, Me, ^{t}Bu; X=^-O_2CR (R=H, Me, Ph, *etc.*))) and type II ([$Mn_3^{III}O$

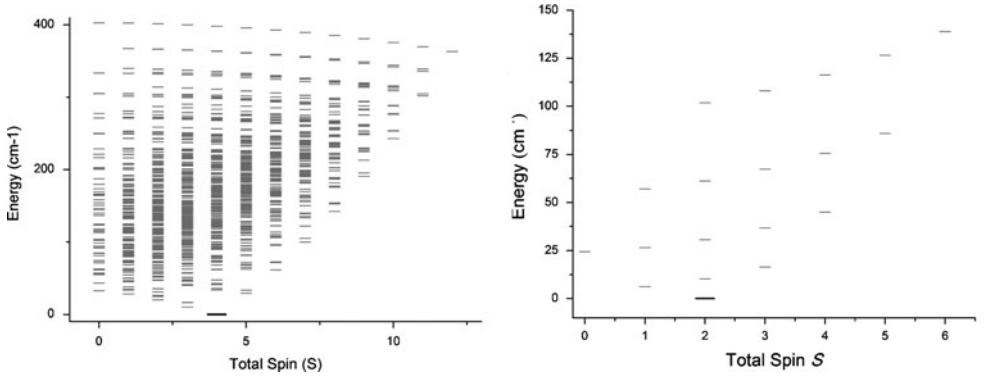

Figure 6. Plot of energy *vs.* total spin (S) state for **1** (left) and **3** (right).

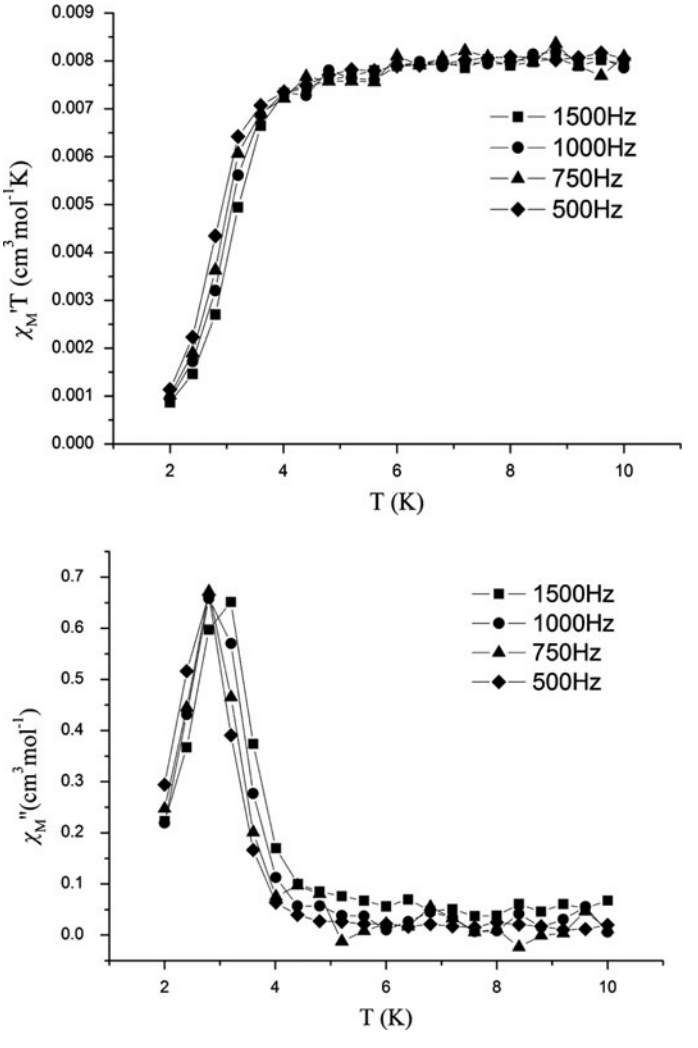

Figure 7. Plot of the in-phase signal $\chi'_M T$ *vs*. T for **2** (top); plot of the out-of-phase χ''_M signal *vs*. T for **2** (bottom).

(R-sao)$_3$(X)(sol)$_{3-5}$] (R=Me,Et, Ph, ^{t}Bu; X=$^-$O$_2$CR (R=H, Me, Ph, etc.); sol=MeOH, EtOH and/or H_2O)) [Mn_3/oximate] clusters [54] in which the carboxylate ligand is found in a bridging *syn,syn*– $\eta^1:\eta^1:\mu$ mode.

Finally, we were not able to fit the magnetic susceptibility data for **2**.

Alternate-current magnetic susceptibility measurements were performed on a polycrystalline sample of **2**, in the 1.8–10 K range in zero applied dc field and 3.5 G ac field oscillating at 500–1500 Hz range, as a means of investigating possible SMM behavior. We chose to measure only **2** as a representative example between **1** and **2**, since it is well established that all $S = 4$ [Mn_6/oximate] clusters display SMM behavior. The in-phase signal, χ'_M, (plotted as $\chi'_M T$ *versus* T in figure 7, top) decreases slightly upon cooling until ~4 K, suggesting the presence of low-lying excited states with S values larger than the ground

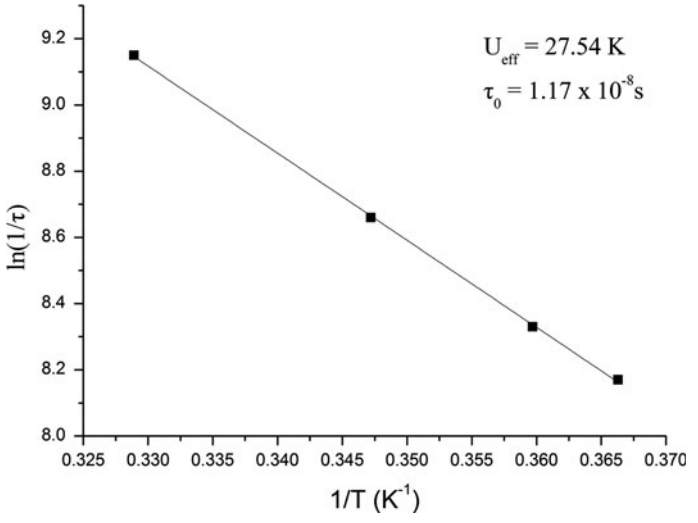

Figure 8. Arrhenius plot using powder ac magnetic susceptibility data for **2**.

state, before it drops rapidly below ~4 K. Extrapolation of the signal above approximately 5–0 K gives a value of ~8 cm^3 K mol^{-1} indicative of an intermediate S ground state ($S \approx 4$). Below ~4 K there is a frequency dependent decrease in the value of $\chi''_M T$ and a concomitant increase in the χ''_M signal. Fully visible frequency-dependent out-of-phase, χ''_M, peaks are observed in a range of frequencies with the peak maximum at 1500 Hz occurring at approximately 3.15 K. The ac powder data were fitted to the Arrhenius relationship (equation (3)),

$$\tau = \tau_0 \exp(U_{\text{eff}}/kT) \tag{3}$$

where U_{eff} is the effective relaxation barrier, τ is the relaxation time, τ_0 is the pre-exponential factor and k is the Boltzmann constant, yielding only one activated regime with $U_{\text{eff}} = 27.54$ K and $\tau_0 = 1.17 \times 10^{-8}$ s (figure 8).

4. Conclusion

In this work, we reported the employment of 5-bromosalicyl aldoximate ligand in manganese chemistry. This new R-saoH_2 oxime ligand carries a bulky substituent on the backbone of the aromatic ring, in contrast with the R-saoH_2 oxime ligands reported so far which carry a bulky group on the oximic carbon atom. In total, three new hexanuclear manganese complexes with the well-known [Mn^{III}_3O(R-sao)$_3$(sol)$_{3-4}$] building block were isolated and characterized. Complexes **1** and **2** display the well-known [Mn_6/oximate] motif, while in **3** the oxocentered trinuclear building blocks are separated by two sodium cations. Magnetic studies for all complexes revealed dominant antiferromagnetic exchanges within the metal clusters, leading to a spin ground state of $S = 4$ for both **1** and **2**, and $S = 2$ for **3**. From

these initial results, two significant conclusions may be drawn: (i) it is not only the bulkiness of the R-substituent of the salicylaldoximate ligand that affects the torsion angles of the Mn–N–O–Mn species, and thus the S of the cluster, but its relevant position with respect to the binding site of the metal ions is of importance as well, and (ii) the "magic area" rule is applicable for this new oxime ligand as well. Currently, work is under way on "transferring" the bulky substituent closer to the metal ring as a means of investigating the limits of its remote effect on the metal ring.

Finally, a brief comparison with the most recently reported work concerning similar hexanuclear oximate manganese clusters [55], shows that: (i) **1** and **2** have spin ground state of $S = 4$, as is the case for the majority of the members of the [Mn_6/oximate] family, (ii) complex **2** displays SMM behavior with U_{eff} value of 27.54 K, close to the U_{eff} values reported for $S = 4$ related molecules, and (iii) **3** displays a unique structural motif in the [Mn_6/oximate] family, with the two building triangular metallic units separated by sodium cations.

Supplementary material

CIF files of complexes **1**–**3**.

Disclosure statement

No potential conflict of interest was reported by the authors.

Funding

This work was supported by the project "IRAKLITOS II – University of Crete" of the Operational Programme for Education and Lifelong Learning 2007–2013 (E.P.E.D.V.M.) of the NSRF (2007–2013), which is co-funded by the European Union (European Social Fund) and National Resources.

References

[1] P. Chaudhuri, M. Hess, E. Rentschler, T. Weyhermüller, U. Flörke. *New J. Chem.*, **22**, 553 (1998).
[2] C.N. Verani, E. Bothe, D. Burdinski, T. Weyhermüller, U. Flörke, P. Chaudhuri. *Eur. J. Inorg. Chem.*, 2161 (2001).
[3] P. Chaudhuri. *Coord. Chem. Rev.*, **243**, 143 (2003).
[4] C.J. Milios, C.P. Raptopoulou, A. Terzis, F. Lloret, R. Vicente, S.P. Perlepes, A. Escuer. *Angew. Chem. Int. Ed. Engl.*, **43**, 210 (2004).
[5] C.J. Milios, A. Vinslava, A.G. Whittaker, S. Parsons, W. Wernsdorfer, G. Christou, S.P. Perlepes, E.K. Brechin. *Inorg. Chem.*, **45**, 5272 (2006).
[6] C.J. Milios, A. Vinslava, P.A. Wood, S. Parsons, W. Wernsdorfer, G. Christou, S.P. Perlepes, E.K. Brechin. *J. Am. Chem. Soc.*, **129**, 8 (2007).
[7] C.J. Milios, A. Vinslava, W. Wernsdorfer, S. Moggach, S. Parsons, S.P. Perlepes, G. Christou, E.K. Brechin. *J. Am. Chem. Soc.*, **129**, 2754 (2007).
[8] C.J. Milios, A. Vinslava, W. Wernsdorfer, A. Prescimone, P.A. Wood, S. Parsons, S.P. Perlepes, G. Christou, E.K. Brechin. *J. Am. Chem. Soc.*, **129**, 6547 (2007).
[9] C.J. Milios, R. Inglis, R. Bagai, W. Wernsdorfer, A. Collins, S. Moggach, S. Parsons, S.P. Perlepes, G. Christou, E.K. Brechin. *Chem. Commun.*, 3476 (2007).
[10] C.J. Milios, R. Inglis, A. Vinslava, R. Bagai, W. Wernsdorfer, S. Parsons, S.P. Perlepes, G. Christou, E.K. Brechin. *J. Am. Chem. Soc.*, **129**, 12505 (2007).
[11] S. Piligkos, J. Bendix, H. Weihe, C.J. Milios, E.K. Brechin. *Dalton Trans.*, 2277 (2008).

[12] U. del Pennino, V. Corradini, R. Biagi, V. De Renzi, F. Moro, D.W. Boukhvalov, G. Panaccione, M. Hochstrasser, C. Carbone, C.J. Milios, E.K. Brechin. *Phys. Rev. B*, **77**, 085419 (2008).
[13] S. Carretta, T. Guidi, P. Santini, G. Amoretti, O. Pieper, B. Lake, J. van Slageren, W. Wernsdorfer, H. Mutka, M. Russina, C.J. Milios, E.K. Brechin. *Phys. Rev. Lett.*, **100**, 157203 (2008).
[14] L.F. Jones, R. Inglis, M.E. Cochrane, K. Mason, A. Collins, S. Parsons, S.P. Perlepes, E.K. Brechin. *Dalton Trans.*, 6205 (2008).
[15] S. Bahr, C.J. Milios, L.F. Jones, E.K. Brechin, V. Mosser, W. Wernsdorfer. *Phys. Rev. B*, **78**, 132401 (2008).
[16] C.P. Raptopoulou, A.K. Boudalis, K.N. Lazarou, V. Psycharis, N. Panopoulos, M. Fardis, G. Diamantopoulos, J.-P. Tuchagues, A. Mari, G. Papavassiliou. *Polyhedron*, **27**, 3575 (2008).
[17] L.F. Jones, M.E. Cochrane, B.D. Koivisto, D.A. Leigh, S.P. Perlepes, W. Wernsdorfer, E.K. Brechin. *Inorg. Chim. Acta*, **361**, 3420 (2008).
[18] S. Datta, E. Bolin, R. Inglis, C.J. Milios, E. Brechin, S. Hill. *Polyhedron*, **28**, 1788 (2009).
[19] C.-I. Yang, K.-H. Cheng, M. Nakano, G.-H. Lee, H.-L. Tsai. *Polyhedron*, **28**, 1842 (2009).
[20] S. Bahr, C.J. Milios, L.F. Jones, E.K. Brechin, V. Mosser, W. Wernsdorfer. *New J. Chem.*, **33**, 1231 (2009).
[21] R. Inglis, L.F. Jones, C.J. Milios, S. Datta, A. Collins, S. Parsons, W. Wernsdorfer, S. Hill, S.P. Perlepes, S. Piligkos, E.K. Brechin. *Dalton Trans.*, 3403 (2009).
[22] E. Cremades, J. Cano, E. Ruiz, G. Rajaraman, C.J. Milios, E.K. Brechin. *Inorg. Chem.*, **48**, 8012 (2009).
[23] J.M. Bradley, A.J. Thomson, R. Inglis, C.J. Milios, E.K. Brechin, S. Piligkos. *Dalton Trans.*, **39**, 9904 (2010).
[24] R. Inglis, S.J. Dalgarno, E.K. Brechin. *Dalton Trans.*, **39**, 4826 (2010).
[25] A.R. Tomsa, J. Martínez-Lillo, Y. Li, L.M. Chamoreau, K. Boubekeur, F. Farias, M.A. Novak, E. Cremades, E. Ruiz, A. Proust, M. Verdaguer, P. Gouzerh. *Chem. Commun.*, **46**, 5106 (2010).
[26] X. Song, R. Liu, S. Zhang, L. Li. *Inorg. Chem. Commun.*, **13**, 828 (2010).
[27] V. Kotzabasaki, R. Inglis, M. Siczek, T. Lis, E.K. Brechin, C.J. Milios. *Dalton Trans.*, **40**, 1693 (2011).
[28] C.-L. Zhou, Z.-M. Wang, B.-W. Wang, S. Gao. *Polyhedron*, **30**, 3279 (2011).
[29] G.-Y. An, A.-L. Cui, H.-Z. Kou. *Inorg. Chem. Commun.*, **14**, 1475 (2011).
[30] R. Inglis, C.J. Milios, L.F. Jones, S. Piligkos, E.K. Brechin. *Chem. Commun.*, **48**, 181 (2012).
[31] X.-T. Liu, J.-X. Li, X. Fei, Q.-L. Wu, B. Yang. *Chin. J. Inorg. Chem.*, **28**, 1234 (2012).
[32] M. Hołyńska, S. Dehnen. *Z. Anorg. Allg. Chem.*, **638**, 763 (2012).
[33] J. Martínez-Lillo, A.R. Tomsa, Y. Li, L.M. Chamoreau, E. Cremades, E. Ruiz, A.L. Barra, A. Proust, M. Verdaguer, P. Gouzerh. *Dalton Trans.*, **41**, 13668 (2012).
[34] G. Novitchi, G. Pilet, D. Luneau. *C.R. Chim.*, **15**, 937 (2012).
[35] J. Martínez-Lillo, L.-M. Chamoreau, A. Proust, M. Verdaguer, P. Gouzerh. *C.R. Chim.*, **15**, 889 (2012).
[36] J. Martínez-Lillo, N. Dolan, E.K. Brechin. *Dalton Trans.*, **42**, 12824 (2013).
[37] C.J. Milios, P.A. Wood, S. Parsons, D. Foguet-Albiol, C. Lampropoulos, G. Christou, S.P. Perlepes, E.K. Brechin. *Inorg. Chim. Acta*, **360**, 3932 (2007).
[38] H.B. Xu, B.W. Wang, F. Pan, Z.M. Wang, S. Gao. *Angew. Chem. Int. Ed. Engl.*, **46**, 7388 (2007).
[39] R. Inglis, L.F. Jones, K. Mason, A. Collins, S.A. Moggach, S. Parsons, S.P. Perlepes, W. Wernsdorfer, E.K. Brechin. *Chem. Eur. J.*, **14**, 9117 (2008).
[40] C.I. Yang, W. Wernsdorfer, K.H. Cheng, M. Nakano, G.H. Lee, H.L. Tsai. *Inorg. Chem.*, **47**, 10184 (2008).
[41] R. Inglis, L.F. Jones, G. Karotsis, A. Collins, S. Parsons, S.P. Perlepes, W. Wernsdorfer, E.K. Brechin. *Chem. Commun.*, 5924 (2008).
[42] R. Inglis, G.S. Papaefstathiou, W. Wernsdorfer, E.K. Brechin. *Aust. J. Chem.*, **62**, 1108 (2009).
[43] C.J. Milios, R. Inglis, L.F. Jones, A. Prescimone, S. Parsons, W. Wernsdorfer, E.K. Brechin. *Dalton Trans.*, 2812 (2009).
[44] C.C. Stoumpos, R. Inglis, G. Karotsis, L.F. Jones, A. Collins, S. Parsons, C.J. Milios, G.S. Papaefstathiou, E.K. Brechin. *Cryst. Growth Des.*, **9**, 24 (2009).
[45] C. Kozoni, E. Manolopoulou, M. Siczek, T. Lis, E.K. Brechin, C.J. Milios. *Dalton Trans*, **39**, 7943 (2010).
[46] E. Manolopoulou, C.C. Stoumpos, M. Siczek, T. Lis, E.K. Brechin, C. J. Milios. *Eur. J. Inorg. Chem*., **2010**, 483 (2010).
[47] C.-I. Yang, P.-Y. Feng, Y.-T. Chen, Y.-J. Tsai, G.-H. Lee, H.-L. Tsai. *Polyhedron*, **30**, 3265 (2011).
[48] M. Hołyńska, N. Frank, S. Dehnen. *Z. Anorg. Allg. Chem.*, **638**, 2248 (2012).
[49] C.-I. Yang, K.-H. Cheng, S.-P. Hung, M. Nakano, H.-L. Tsai. *Polyhedron*, **30**, 3272 (2011).
[50] L.-L. Li, S.-N. Wang, J. Lu, F.A.N. Cao, L.-Q. Kong, J.-M. Dou, D.-C. Li. *J. Coord. Chem.*, **66**, 306 (2013).
[51] W.R. Dunstan, T.A. Henry. *J. Chem. Soc.*, **75**, 66 (1899).
[52] G.M. Sheldrick. *Acta Crystallogr., Sect. A*, **64**, 112 (2008).
[53] N.F. Chilton, R.P. Anderson, L.D. Turner, A. Soncini, K.S. Murray. *J. Comput. Chem.*, **34**, 1164 (2013).
[54] R. Inglis, S.M. Taylor, L.F. Jones, G.S. Papaefstathiou, S.P. Perlepes, S. Datta, S. Hill, W. Wernsdorfer, E.K. Brechin. *Dalton Trans.*, 9157 (2009).
[55] A. Perivolaris, A.M. Fidelli, R. Inglis, V.G. Kessler, A.M.Z. Slawin, E.K. Brechin, G.S. Papaefstathiou. *J. Coord. Chem.*, **67**, 3972 (2014).